Article

3D hierarchical aquaporin-like nanoporous graphene membrane with engineered tripartite nanochannels for efficient oil/water separation

Check for updates

Hanaa M. Hegab [1,3] ✉, Ahmed Elmekawy [1,3], Cyril Aubry[2], Parashuram Kallem[1], Vijay S. Wadi[1], Fawzi Banat[1] & Shadi W. Hasan [1] ✉

The aqueous system is being polluted by the untreated direct discharge of industrial oily wastewater into the ecosystem. Due to its low cost, energy economy, and sustainability, the advanced membrane filtration method is regarded as one of the best methods for treating oily wastewater. Its exceptional atomic thickness and superior amphiphilic properties of graphene oxide (GO) nanosheet make it one of the finest 2D constituents for creating membranes with high permeability. Nevertheless, the interlayer d-spacing of multi-stacked GO membranes is crucial since it is responsible for the permeability/selectivity trade-off. To efficiently separate oil-in-water emulsion using an in-situ polymerization technique, we developed an aquaporin-like 3D hierarchical multi-functionalized nanoporous graphene (NPG) membrane with tripartite nanochannels. The extraordinary, prepared membrane displayed both ultra-water-permeability of 2490 L m^{-2} h^{-1}.bar along with superior selectivity. Consequently, the permeance of the aquaporin-like 3D hierarchical multi-functionalized NPG membrane achieves a higher flux than the GO membrane, while the oil rejection reaches ~97%.

The intensifying industrial activity and the high population growth resulted in the global growth of urbanization, putting pressure on clean water demands and leading to substantial common freshwater supply shortages. Wastewater contaminated with oil, normally produced by several industrial sectors, has become a serious daily environmental issue. Oil/water nano-emulsions (stabilized by surfactants), with droplet sizes 20–200 nm, are generally produced by different industries, i.e., cosmetics, oil refineries, food, and pharmaceutical[1,2]. These nano-emulsions led to several health and environmental issues due to their high stability and conveyance in the environment[3], causing serious eco-toxicity because of the surfactants' powerful biological reactivity[4,5].

The oil/water nano-emulsion separation process is still challenging because of the co-occurrence of small surfactant molecules along with nano-oil droplets[6]. The conventional technologies (i.e., gravity separation, skimming, air flotation, and centrifugation) are still not functional in the efficient removal of surfactant/emulsified oil from the nano-emulsion[7]. Based on the size exclusion principle, the membrane is one of the most encouraging

technologies to tackle the challenge of nano-emulsion separation, with recent studies showing significant progress regarding separation efficiency[8]. One example of these achievements is the study conducted by Solomon et al. in which a hydrophobic membrane was employed in the separation process of water-in-oil nano-emulsion, supporting the passage of oil and repulsion of water by the membrane[9]. However, hydrophobic membranes possess some challenges regarding the low flux of the viscous oil (Hagen–Poiseuille equation), and oil fouling due to the membrane hydrophobicity[10,11]. These challenges gave the advantage to alternative research directions to employ hydrophilic membranes for the oil-in-water separation.

On its border and basal plane, graphene oxide (GO) comprises a significant amount of oxygenic reactive groups. It also possesses unique features, i.e., an accessible interface, great surface area, and ultrafast shuttling properties[12–15]. It was earlier discovered in 2007 that paper-like GO-based membranes had selectivity potential. Water can travel through the GO-based membranes' wrinkled interlayer space and sheets with nanochannels all over them, while other molecules larger than the distance between

[1]Center for Membranes and Advanced Water Technology (CMAT), Department of Chemical Engineering, Khalifa University of Science and Technology, PO Box, 127788 Abu Dhabi, United Arab Emirates. [2]Research Laboratories Operations, Khalifa University of Science and Technology, PO Box, 127788 Abu Dhabi, United Arab Emirates. [3]These authors contributed equally: Hanaa M. Hegab, Ahmed Elmekawy. ✉e-mail: hanaa.hegab@ku.ac.ae; shadi.hasan@ku.ac.ae

adjacent GO nanosheets are effectively blocked[16]. Additionally, the hydrophilic properties of GO make it possible to fabricate membranes for the separation of oil-in-water emulsions. Accordingly, several GO-coated membranes have been fabricated for this purpose, i.e., sulfonated GO/TiO$_2$ spheres[17], GO/Al$_2$O$_3$ microfiltration (MF)[18], and GO ultrafiltration (UF) membranes, showing efficient separation capacity. Nevertheless, the instability of GO membranes fabricated using porous MF support was reported owing to the weak interaction with the supporting surface, resulting in the development of crinkles and detachment from the surface[19]. To overcome this challenge, different types of polymeric materials functionalized with carbon-based nanomaterials were reported to enhance the stability of fabricated membranes[20,21].

The interlayer spacing is amongst the most crucial regulating features with high separation performance GO-based membranes and is essential for the interpolation of ions, nanomaterials, or molecules among adjacent GO nanosheets. This parameter is critical in the determination of the separation capacity of GO-based membranes, permitting the passage of some species and rejecting others[22]. The challenging part of this approach is the degree of accuracy to establish water-stable interlayer spacing. Another obstacle is overcoming the resistance associated with high mass shuttling, where molecules traveling through a graphene (Gr)-based membrane should find a way around the encompassed nanosheets, resulting in lengthy transferring channels, therefore reducing the membrane permeance.

The biological cell membrane, which is made up of proteins, lipids, and hydrophilic polymers, functions as a wall separating the interior of the cell from its external world, providing security and regulating the flow of molecules and ions out and into the cell[23]. Aquaporin proteins are the core component of the cell membrane, functioning as regulating channels for the flow of water, ions, and various solutes due to their hydrophobic nature. Moreover, the scarcity of water binding sites in aquaporins accelerates water transport, and the availability of ion binding sites and steric effects contribute towards the efficient transport control of ions and solutes[24]. In addition, the steric barrier and the development of a surface layer of repulsive hydration on the cell membrane are some of the processes by which the brush-shaped hydrophilic polymers of the cell membrane can act as a shield.

Herein, we engineered a facile approach to fabricate an aquaporin-like 3D hierarchical multi-functionalized nanoporous graphene (NPG) membrane with tripartite nanochannels using an in-situ polymerization/vacuum-assisted strategy. Because of the reduced length of the mass passageways, which results in elevated permeance, and the existence of expansive/constricted interlayer nanochannels, which ensure exceptional selectivity, the distributed pores in NPG nanosheets gave direct nanochannels. The created membrane outperformed the permeance/rejection trade-off conflict to successfully purify surfactant stabilized oil/water emulsion.

Results and discussion
Synthesis and characterizations of GO and NPG nanosheets
While NPG nanosheets were produced using an oxidative etching technique using a combined H$_2$O$_2$ and NH$_3$ solution, GO nanosheets were produced through chemical oxidation along with graphite exfoliation (Fig. 1). To control the porosity of the GO nanosheets, the unstable oxidized sp^3 portions were etched during the first hour of the reaction[25,26]. The TEM morphologies of GO and NPG are illustrated in Fig. 2a, in which the synthesis of nanosheets was confirmed by the presence of wrinkled GO with lateral sizes ranging from 0.5–1 μm. Furthermore, nanopores were visualized on the NPG nanosheets using the high-resolution TEM (HR-TEM) with a minimum pore size of 11.3 ± 0.4 and a maximum of 20 ± 3 nm after utilizing the 60 min etching time (Fig. 2c).

Moreover, the occurrence of single-layer GO along with NPG nanosheets was verified by examining their topographies via AFM. The GO
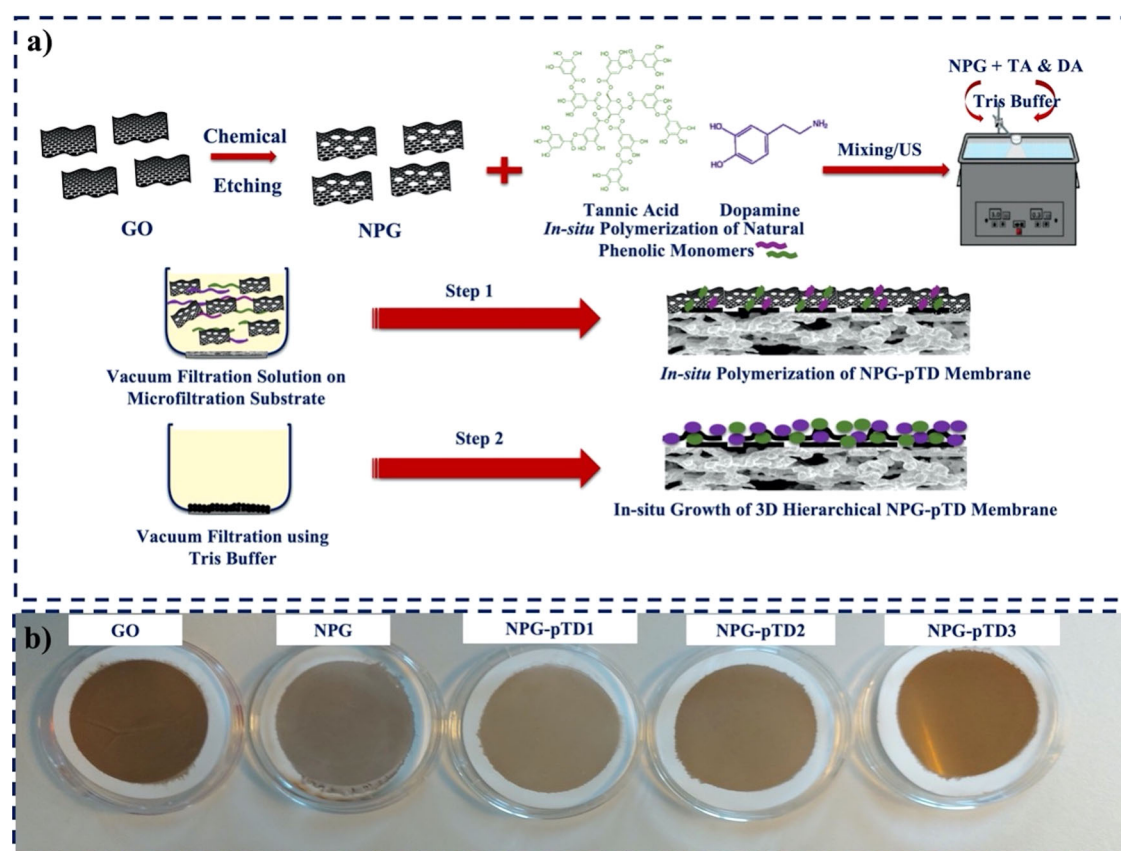

Fig. 1 | Preparation procedures. Illustrative diagram showing the preparation of NPG nanosheets and membranes, in which **a** explains the method to synthesize NPG nanosheets using vacuum filtration technology, and **b** illustrates an actual photo of fabricated membranes.

Fig. 2 | Morphological and topographical analyses of nanomaterials. Surface examinations of GO and NPG, where **a** represents the TEM image of prepared GO nanosheets, **b** exemplifies the AFM image of GO nanosheets, with their height profile, **c** shows the TEM image of the synthesized NPG nanosheets, and **d** demonstrates the AFM visualization of NPG nanosheets, including their pores and height profiles.
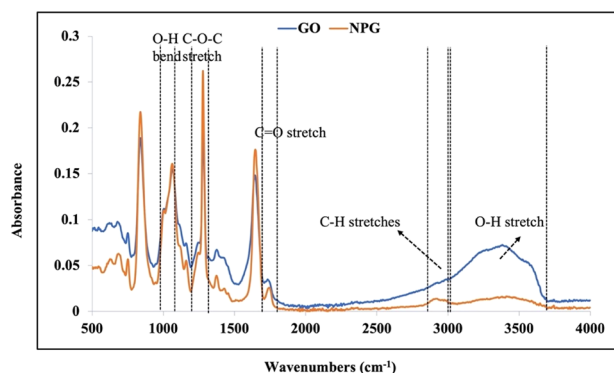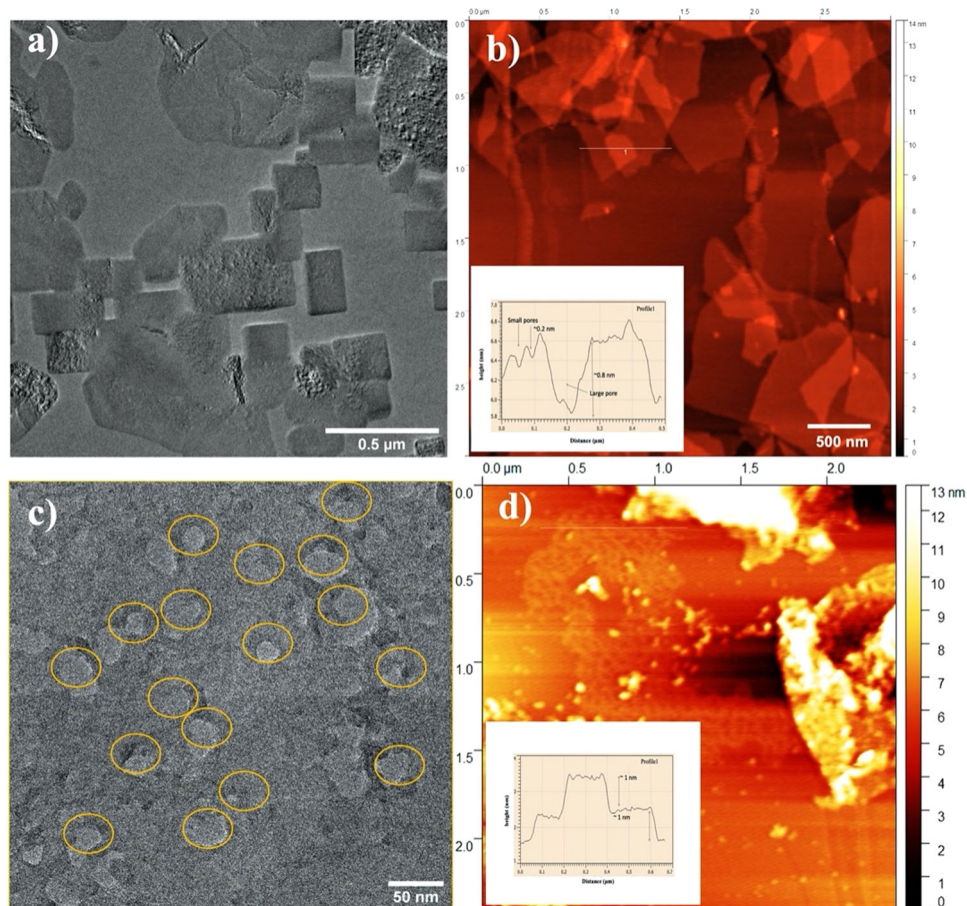

Fig. 3 | FTIR surface chemical analysis of nanomaterials. FTIR spectra of GO and NPG membranes.

nanosheets were confirmed to be non-porous with a thickness of 1.25 nm (Fig. 2b). The nanosheets' lateral size was noticed to be uniform and in the range of 500–1000 nm. Oppositely, the NPG nanosheets were observed to have a small pore size (11–20 nm) and a thickness of 0.8 nm (Fig. 2d). Because of the existence of –COC, –OH, and C = O groups, the GO nanosheets exhibited a negative zeta potential (-45.2 ± 0.9 mV)[27]. Prior to etching, the net charge of the NPG shifted to -2.3 ± 0.2 mV, which is regarded as additional proof of the fractional reduction of NPG by means of NH_3 (Fig. 3).

FTIR spectra displayed the distinctive functional groups related to GO (Fig. 3), showing O–H stretching peaks (3750–3000 cm^{-1}), asymmetric and symmetric C–H stretching peaks (3000 and 2850 cm^{-1}), and C = O stretching peaks (1747 cm^{-1}). Additionally, the peak at 1250 cm^{-1} indicates

the presence of the O–C–O stretch, and the O–H bend was indicated at 1025 cm^{-1}. NPG nanosheets showed identical peaks and functional groups in the same range, except for the decrease noted in the intensity of the peak in the range of 3750–3000 cm^{-1}, which indicated the occurrence of partial reduction.

The OH ratio was significantly diminished compared to that of pure GO. The amino fractions are attached to the NPG sheets under the alkalinity of NH_3 through the SN2 nucleophilic dislocation interaction of the GO's functional groups of epoxy with NH_3[28,29]. The C–H stretching peak's weakness was also seen in the NPG spectrum, and this can be attributed to the fact that NPG is made mainly by ordered chemical etching, which creates holes, followed by partial reduction[30]. The results stated above confirmed that the GO was successfully synthesized and oxidized, and the NPG nanosheets were successfully etched. The obtained FTIR spectrum of the synthesized nanomaterials is in agreement with previous studies[31–35].

Fabrication of the 3D hierarchical NPG-pTD$_X$ membranes
The preparation method used to fabricate the aquaporin-like 3D hierarchical NPG-pTDX membranes included chemically etching the GO nanosheets, multi-functionalizing the NPG nanosheets, preparing the GO, NPG, and NPG-pTDX membranes using a common vacuum filtration technique, and post-treating the NPG-pTDX membranes with tris buffer solution (Fig. 1a). DA is a type of biologically adaptive chemical that has functional groups binding catechol and primary amines. DA was able to in situ polymerize and assemble spontaneously in an alkaline environment to create a polydopamine (pDA) layer that was able to adhere to all types of substrates through covalent and non-covalent reactions[36–39] in contrast to some other polymer composite materials. Additionally, at alkaline pH

Fig. 4 | FTIR surface chemical analysis of membranes. a The FTIR spectra of different fabricated membranes and **b** their magnified distinctive peaks.
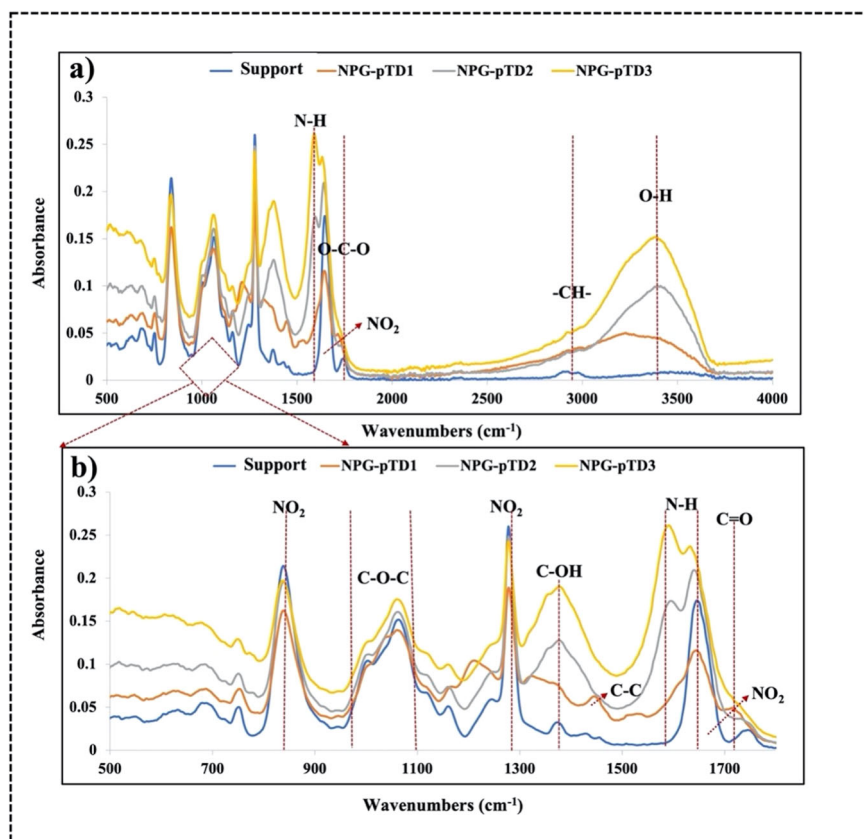
conditions, in-situ self-polymerization can also deposit polyphenols like (TA) on the surfaces of substrates[40]. Throughout the adjusted synthesis method, TA and DA were mixed with NPG (0.02 mg mL^{-1}) in tris buffer without adjustment of pH to control the in-situ self-polymerization of different phenolic groups. Through hydrogen bonding and π–π stacking, the protonated TA and DA adhered to the oxygen functional groups of NPG. The mixture was stirred to obtain a uniform spreading of TA and DA within the NPG nanosheets and was subsequently filtered with various loadings on the top of the support. Multi-functionalized NPG nanosheets with the loading of 71 µg cm^{-2} homogeneously covered the porous support without leaving any flaws (Fig. 1b). The fabricated membrane was coded as NPG-pTD$_X$, obtained after the completion of the in-situ self-polymerization with tris buffer (pH 8.5) different membranes with various loadings (NPG-pTD$_1$, NPG-pTD$_2$, and NPG-pTD$_3$). The in-situ development of multifunctionalized polyphenolic nanoparticles can be achieved on the surface as well as through the interlayer d-spacing of the NPG nanosheets using TA and DA as phenolic precursors. The prepared membranes showed the brown and gray colors of GO and NPG control membranes, respectively (Fig. 1b), while the different partially reduced membranes (NPG-pTD$_1$, NPG-pTD$_2$, and NPG-pTD$_3$) displayed a brown color gradually getting darker in proportion to loading.

Characterizations of the 3D hierarchical NPG-pTDX membranes
ATR-FTIR tests were carried out to define the chemical functional groups on the surface of the prepared membranes. The FTIR spectra of the support and NPG-pTD1, NPG-pTD2, and NPG-pTD3 membranes are presented in Fig. 4a, b. The FTIR spectra of three intense bands observed in the case of the nitrocellulose mixed ester membrane (support), which is attributed to various nitrate group vibrations. These peaks appeared at wavelengths 840, 1280, and 1660 cm^{-1}, corresponding to the valence NO stretching, symmetric NO$_2$ stretching, and antisymmetric NO$_2$ stretching, respectively[41]. Moreover, the typical peaks at 1800 and 1000 cm^{-1} correspond to the

carbonyl C = O and O–C–O groups of the ester, while the existence of the C–H stretching peak was detected between 2850 and 3000 cm^{-1} [42].

The in situ self-polymerization of TA and DA-based NPG membranes, including N–H and O–H groups can be observed in the FTIR spectrum presented in Fig. 4a, b. Relative to support, the FT-IR spectra of NPG-pTD1, NPG-pTD2, and NPG-pTD3 membranes have similar peaks besides the huge augmentation of O–H stretching vibrations at 3430 cm^{-1} as the loading of used pTD-NPG increased and shifting C = O group to 1710 cm^{-1} and the existence of a new peak of CON-H shown in the range of 1600–1650 cm^{-1}. This confirms the hydrogen bonding and π–π stacking formation between the protonated pTA and NPG, in addition to the creation of covalent bonds among pDA and oxygen functional groups of NPG nanosheets, which is beneficial to graft NPG nanosheets onto the surface of support for the successful fabrication of the stable 3D hierarchical NPG-pTDX membranes[43,44].

Figure 5 displays the prepared membranes' hydrophilicity profile. Water contact angles (WCAs) of 35.5° and 45.8° for GO and NPG membranes, respectively, are attributed to the occurrence of more hydrophilic oxygen-reactive groups in the former. The NPG membrane displayed less hydrophilicity due to the major changes in its morphological feature, along with a partial reduction of NPG nanosheets. The wettability profiles of the NPG-pTD1, NPG-pTD2, and NPG-pTD3 membranes were interestingly enhanced as the concentration of utilized NPG-pTD increased, compared to GO and NPG membranes. The results confirm the successful creation of hydrophilic 3D hierarchical NPG-pTDx-based membranes, with more hydrophilic –NH, C = O and –OH functional groups on the fabricated membranes' surface.

The SEM was used to visualize the surface morphology of the support, NPG, and the aquaporin-like 3D hierarchical NPG-pTDX membranes. As shown in Fig. 6, the successful preparation of the NPG and the aquaporin-like 3D hierarchical NPG-pTDX membranes was confirmed. The vacuum filtration technique achieved the full coverage of microporous support using

various loadings of NPG and NPG-pTD nanosheets. The SEM images of NPG and NPG-pTD1 membranes displayed a wrinkled surface due to the interlayer interactions between the NPG or NPG-pTD nanosheets during the fabrication process[45]. The higher loadings of used NPG-pTD in NPG-pTD2 and NPG-pTD3 membranes resulted in the formation of self-assembled 3D hierarchical nanoparticles on the surface via the in-plane interactions. Furthermore, the higher magnification of captured SEM images of the fabricated NPG-pTD2 and NPG-pTD3 membranes proved the formation of self-assembled 3D hierarchical nanoparticles through the in-situ self-polymerization approach, in which the nanoparticles a size between 5 and 7 nm. Unlike, the higher magnification SEM images of the NPG and NPG-pTD1 membranes showed the nonexistence of 3D hierarchical nanoparticles.

The cross-sectional visualization of the support verified the absence of a dense top layer, while the NPG, NPG-pTD1, NPG-pTD2, and NPG-pTD3 membranes displayed a dense layer with different thicknesses of 211, 386, 535, and 611 nm, respectively, according to the loading increase of utilized NPG-pTD nanosheets (Fig. 7). The SEM images verified that there was no negative impact on the creation of an identical laminar layer on the top of membranes through the in situ growth of self-assembled 3D hierarchical NPG-pTD1. Additionally, according to the AFM analysis, a single NPG nano-layer measured 0.8 nm in width (Fig. 2). Accordingly, the cross-sectional SEM images of NPG and NPG-pTD1 showed that there were ~265 and ~485 nano-layers, respectively. Although using the same loading of NPG and M-NPG, the thickness of the NPG-pTD1 membrane increased by 1.8 times compared to the NPG membrane, which is ascribed to the successful in-situ growth of self-assembled 3D hierarchical pTD1 nanoparticles among the nanosheets of NPG. Additionally, the EDS mapping of the fabricated membranes' surfaces was completed to analyze the elemental compositions as presented in Fig. 6. The EDS mapping confirmed the occurrence of C, O, and N in all membranes. The distribution and intensity of this O and N enhanced in NPG-pTD1, NPG-pTD2, and NPG-pTD3 membranes, which can be attributed to the successful intercalation with DA and TA.
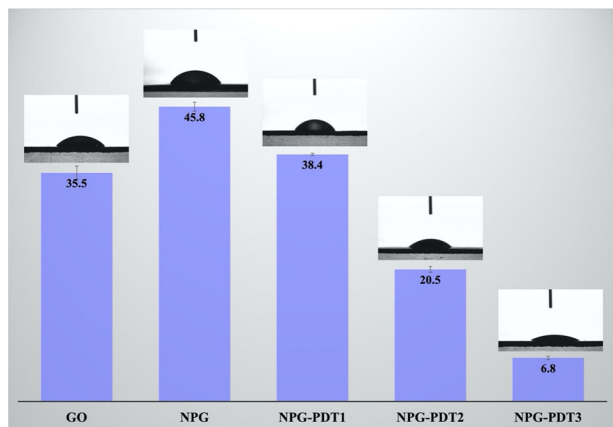

Fig. 5 | Surface wettability analyses. Contact angle profiles of fabricated membranes. Error bars represent the standard deviation for five measurements.
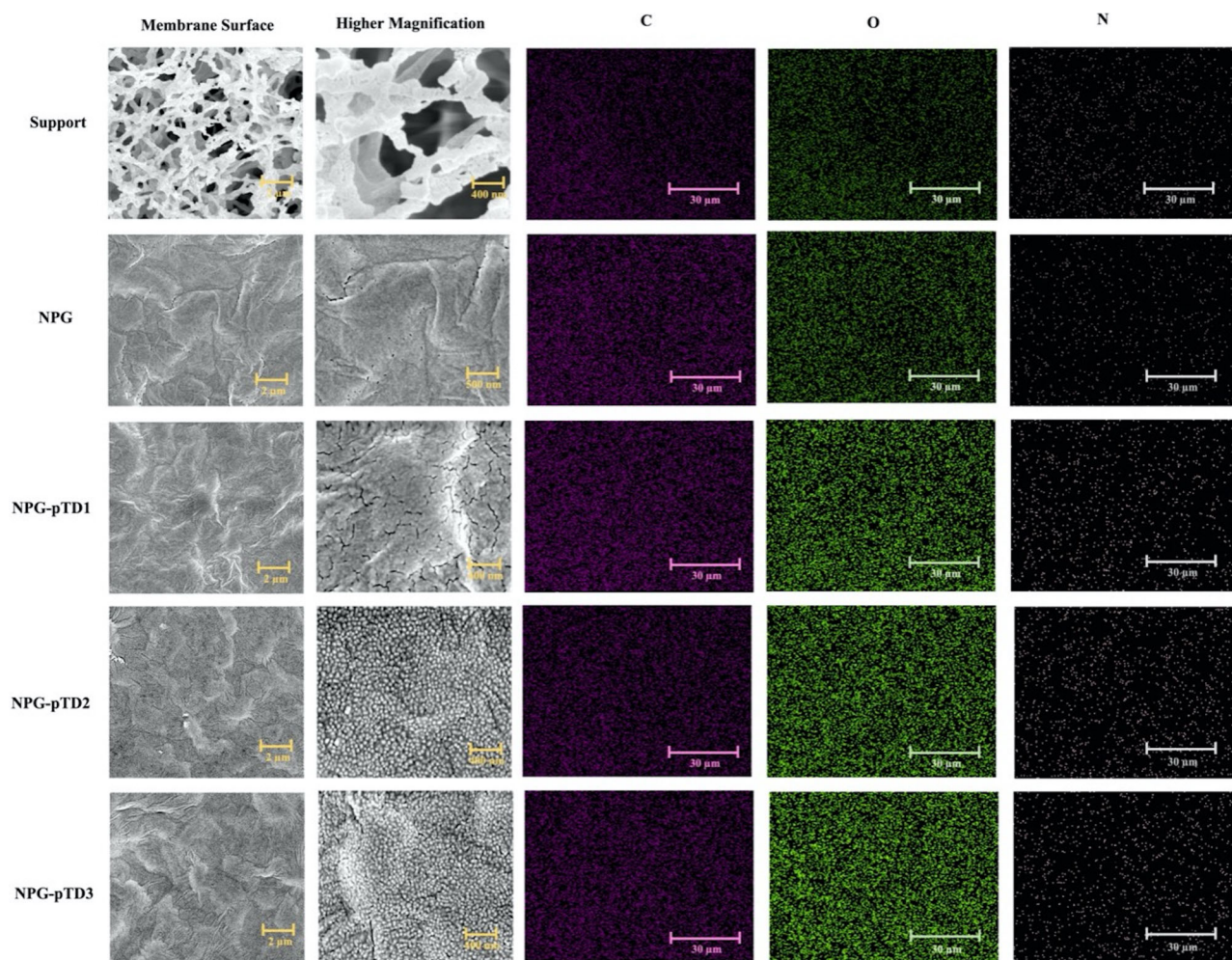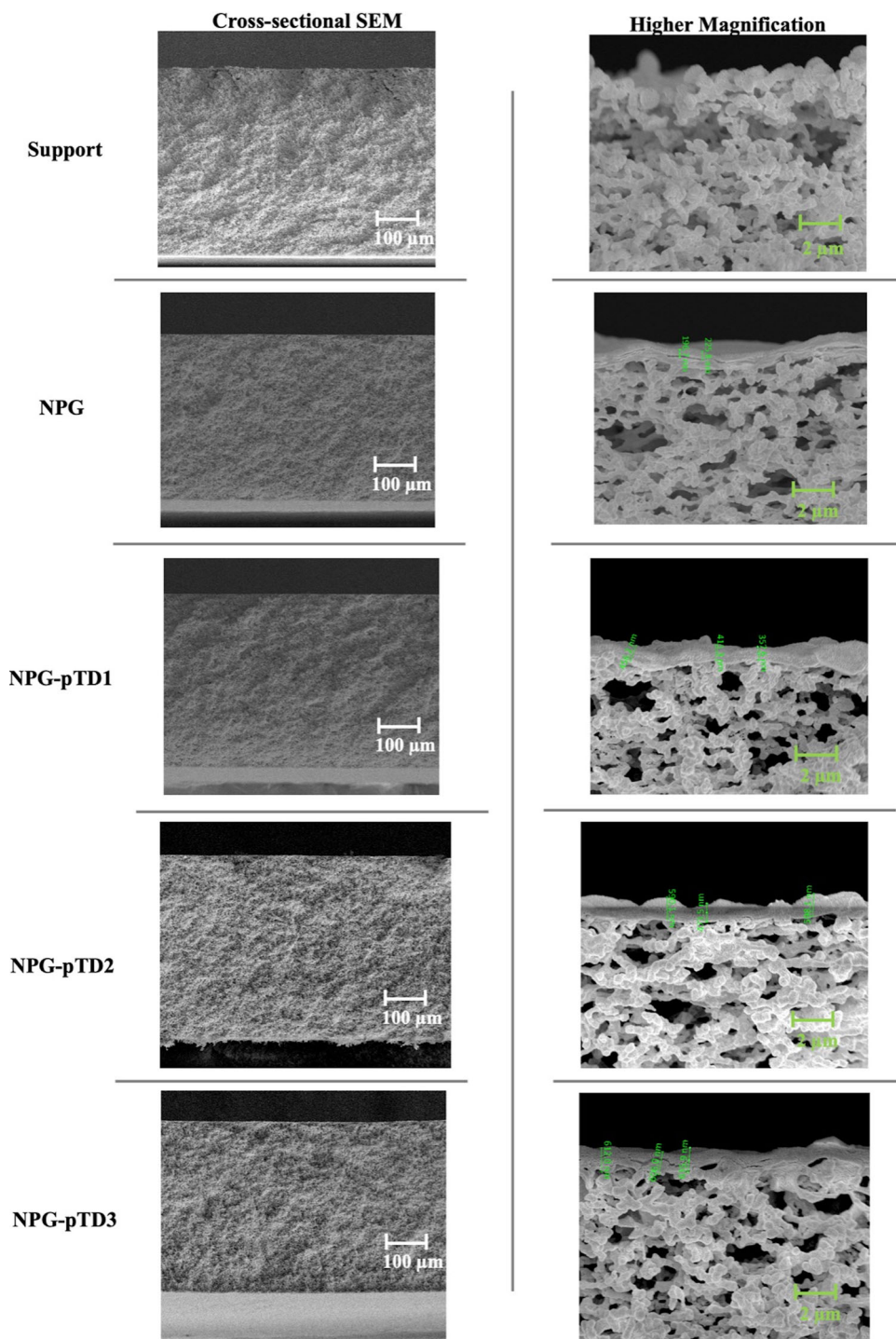

Fig. 6 | Morphological structure and elemental analyses. SEM images of support and prepared membranes and their EDS surface elemental mapping.

Fig. 7 | Morphological analyses. The SEM cross-sectional images of synthesized membranes.

The fabrication approach encompasses two phases: initially, the adherence of DA and TA molecules within the NPG nanosheets via π–π stacking, along with hydrogen bonding; hence, the protonated TA and DA can attach to the oxygen functional groups of NPG. In the second stage, a complete in situ polymerization reaction results in the growth of self-assembled 3D hierarchical NPG-pTD after treatment with an adjusted tris buffer solution. This unique morphological structure of prepared membranes enhanced the d-spacing from 0.8 to 0.95 nm due to the formation of aquaporin-like channels. The membrane's efficiency, in terms of selectivity and flux, is controlled by the d-spacing among the NPG and M-NPG nanosheets; in this study, aquaporin-like engineered channels with alternative arrangements were able to achieve both excellent permeability and high selectivity (Fig. 8). The XRD pattern of all NPG, NPG-pTD1, and NPG-pTD2 membranes included d-spacing of 0.8, 0.79, and 0.75 nm according to Bragg's law[30], while the NPG-pTD3 membrane exhibited a wider d-spacing of 0.95 nm and tight one of 0.69 nm, which can be attributed to the presence of attached self-assembled 3D hierarchical NPG-pTD after treatment with adjusted tris buffer solution (Fig. 8). The output is consistent with the results of the SEM cross-sectional and surface analyses.

3D hierarchical NPG-pTDX membranes: performance assessment

The performance of GO, NPG, and the 3D hierarchical NPG-pTDX membranes was assessed via vacuum filtration using water emulsions with
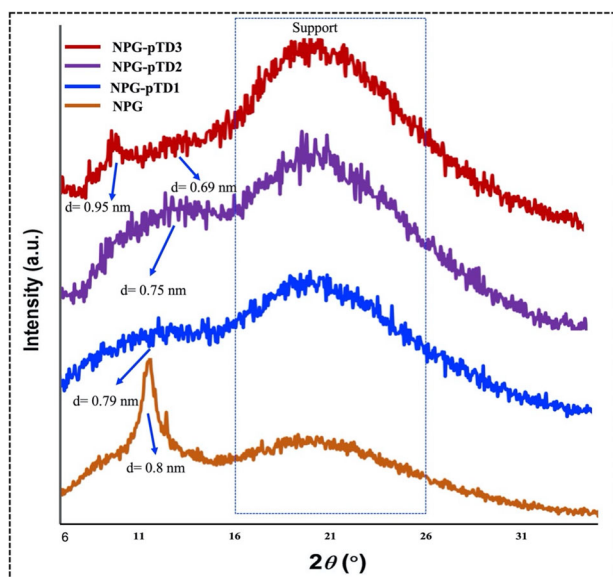
Fig. 8 | Crystallographic structure. XRD analysis of fabricated membranes.

Fig. 9 | Performance profiles of fabricated membranes. Flux and removal capacity of the fabricated membranes for oil/water emulsion. Error bars represent the standard deviation for three experiments.

surfactant-stabilized oil (Fig. 9). The fabricated GO membrane exhibited 74% oil in water separation, compared to the NPG membrane has only 50% removal capacity. The permeability performance of GO and NPG membranes was almost 313 and 870 L m^{-2} h^{-1} bar, respectively. The permeability of the GO membrane can be ascribed to the attraction of water to the hydrophilic oxygen reactive groups region of GO nanosheets passing quickly through the hydrophobic graphitic region with almost no resistance[16]. While the key mechanism of the GO membrane's selectivity is ascribed to d-spacing among the stacked nanosheets, which is tighter than the size of the oil nano-emulsion[46], the swelling issue of GO nanosheets could be the reason for less rejection efficiency.

The NPG membrane was integrated with nanohole arrays (~11 to ~20 nm) and distributed through the nanosheet exterior (Fig. 2). The rejection capacity of the NPG membrane was less than that of the GO membrane. Nevertheless, the water penetrability across the NPG membrane is almost 2.8 times that of the GO membrane, which is ascribed to the combination between direct nanochannels via nanoholes distributed in the nanosheets, along with the d-spacing nanochannels among stacked nanosheets. The d-spacing nanochannels in the nanosheets of 2D membranes are important as they control the separation and permeability efficiencies. However, the 2D membranes suffer from permeability/selectivity trade-off challenges. To address this bottleneck, we engineered the 3D hierarchical aquaporin-like NPG-pTDX membranes with tripartite nanochannels comprising expansive-compact alternative d-spacing nanochannels intercalated with pTD nanoparticles plus the nanochannels of NPG nanosheets.

The oil removal abilities of the NPG-pTD1, NPG-pTD2, and NPG-pTD3 membranes were 73, 84, and 97%, while the permeabilities profile interestingly increases with almost values of 1000, 1244, and 2490 L m^{-2} h^{-1} bar, correspondingly (Fig. 9). The results confirmed the increment of the permeability of membranes as the loading of the hydrophilic pTD increased, which is in agreement with contact angle analysis (Fig. 5). The aquaporin-like NPG-pTD3 membrane had a superior oil removal and ultra-high permeability relative to the other membranes with more than 8 times the permeability of the GO membrane, which is ascribed to the growth of the hydrophilic 3D hierarchical pTD among the NPG nanosheets as shown in Figs. 6 and 10. The mechanism of efficient oil removal can be elucidated through the development of a thin water-solid interface layer on the surface of the NPG-pTD3 membrane, which works perfectly to block oil adhesion. The highly uniform self-assembly distribution of the hydrophilic 3D pTD amid the NPG nanosheets through in-situ polymerization reactions
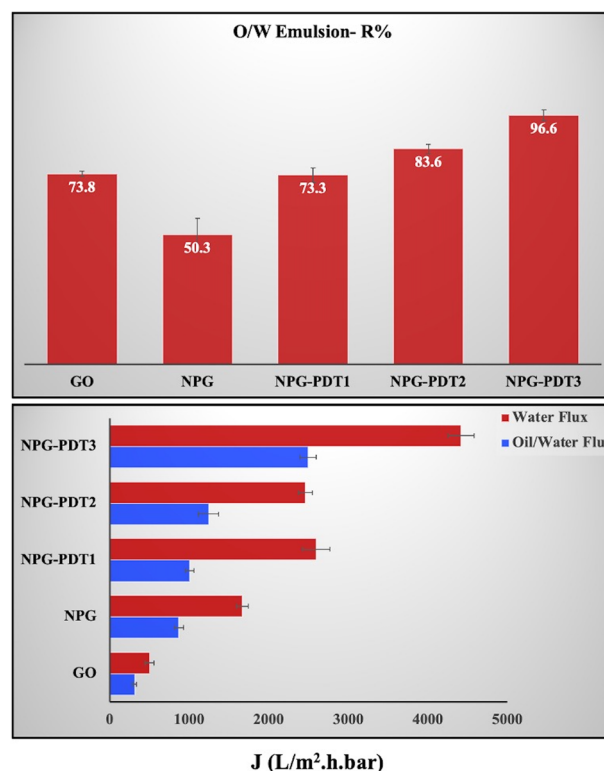
generates wide hydrophilic d-spacing regions alternative with tight hydrophobic graphitic regions, which can be considered a key role in oil/water separation (Fig. 10). Table 1 compares NPG-pTD membrane with the most recent research on oil-water separation membranes[12,13,47–51]. The outcomes demonstrated that, without sacrificing rejection capacity, the NPG-pTD membrane reported the highest flux, which is 2–27 times greater than the state-of-the-art membranes in the literature. This result demonstrates the distinctive structure of the aquaporin-like NPG-pTD membrane with tripartite nanochannels, allowing the development of an ultra-permeable membrane for oil–water separation and overcoming the trade-off between permeability and selectivity.

The reusability evaluation of NPG-pTD3
One significant factor that contributes to membrane durability in practical applications is reusability. The aquaporin-like NPG-pTD3 membrane exhibited superior oil removal and ultra-high permeability in this study compared to the other membranes, so it was chosen to be evaluated to separate oil-in-water emulsions under vacuum filtration for four cycles. Following each emulsion filtration operation, the membrane surface was washed with deionized water. The results are displayed in Fig. 11, and it can be observed that the flux decreased gradually as the filtering cycle increased, while the overall oil removal remained almost similar. The NPG-pTD3 demonstrated good stability and reusability during the extended filtration process.

The outcome verifies that the 3D hierarchical aquaporin-like NPG-pTDX membranes with tripartite nanochannels were successfully prepared, enabling high performance and overcoming the flux/selectivity trade-off. Interestingly, the NPG-pTD3 membrane showed ultra-high permeability of 2490 L m^{-2} h^{-1} bar, along with high oil rejection of more than 96%. The practical in situ polymerization method allowed the formation of expansive/compact alternative d-spacing nanochannels to tailor the chemical and physical structure of the prepared membranes. These engineered membranes feature a one-of-a-kind pattern of an aquaporin-like multi-
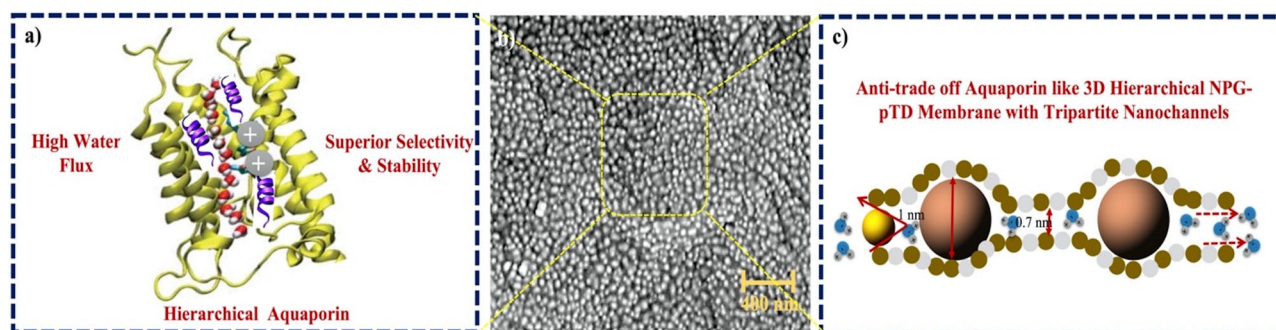
Fig. 10 | Mechanism of the performance enhancement. Descriptive illustration to unwrap the design concept of the aquaporin-like 3D hierarchical NPG-pTDX membrane. **a** Graphic diagram portrays the unique feature of the aquaporin channel. **b** SEM image of the aquaporin-like 3D hierarchical NPG-pTD membrane. **c** Schematic figure to reveal the design of tripartite nanochannels.

functionalized NPG that has tremendous potential for treating oily waste-water from different industries.

Methods

Materials

All chemicals were obtained from Sigma-Aldrich™: graphite powder with a size of 10 mesh, phosphoric acid (H_3PO_4, 85%), sulfuric acid (H_2SO_4, 96%), hydrochloric acid (HCl, 36%), ethanol (95%), H_2O_2 (35%), potassium permanganate ($KMnO_4$, 99%), ammonium hydroxide solution (NH_4OH), sodium hydroxide, tris buffer, dopamine hydrochloride (DA, $C_8H_{11}NO_2 \cdot$ HCl, 98%) and tannic acid (TA, $C_{76}H_{52}O_{46}$). Advantec provided the 0.22 micron, 47 mm diameter nitrocellulose mixed ester MF support used in this study, and widely available vegetable oil was also used. A purification device was used to provide the deionized (DI) water (Millipore Milli-Q Plus 185–15 MΩ cm at 25 °C).

GO nanosheets synthesis

The preparation of GO nanosheets was carried out using the simplified method of Hummer from graphite flakes[52]. In brief, the flakes, along with $KMnO_4$ (1:6), were cautiously added to the H_2SO_4/H_3PO_4 solution (1:9) in an ice bath to keep the exothermic reaction under control. Complete oxidation was accomplished by stirring the mixture for 72 h at 35 °C before it was placed once more in an ice bath. Afterward, the mixed solution was steadily diluted with two amounts of DI water: 250 mL at <35 °C and 500 mL. H_2O_2 solution (35%) was cautiously added to stop the reaction by removing the unreacted $KMnO_4$. The supernatant was removed after

filtering the produced solution. To achieve a pH of 6.8, the gathered GO was washed with HCl solution and DI water. By ultrasonically distributing the GO yield in DI water, it was then kept.

Fabrication of NPG-modified nanosheets

NPG was prepared from the synthesized GO dispersion (~2 mg mL⁻¹). The H_2O_2 and NH_4OH mixture was gradually introduced to the GO dispersion (5:5:1). To finish the etching process; the mixture solution was then kept in an oil bath (55 °C) with magnetic stirring at 30 rpm for 1 h. The etched GO solution was subjected to centrifugation at 12,000 rpm (90 min) to separate the leftover reactants and products, and the supernatant was discarded. To produce a single-layered, uniformly sized NPG, the resulting dispersion was centrifuged again at 3000 rpm for 10 min to remove unexfoliated and noticeably large NPG sheets. The diluted precipitate with tris buffer was then ultrasonicated after the addition of DA and TA. In order to facilitate the attachment of DA and TA on NPG nanosheets with a final ratio of 50: 50: 0.5, respectively, the combination was then stirred for 20 min at room temperature.

Synthesis of membranes

Utilizing GO and NPG (71 µg cm⁻²) along with various concentrations (71, 142, and 212 µg cm⁻²) of the multifunctional NPG solution on the surface of microfiltration support, the fabrication of membranes was done using the vacuum filtration technique (Fig. 1). Since the membranes were NPG-pTDX-coded, the character "X" stands for the various loadings. The support was soaked in DI water prior to the deposition process. The amount of NPG or multifunctional NPG in the solution and the coating area were used to calculate the coating layer thickness. Finally, 10 mL tris buffer solution (10 mM, pH 8.5) was filtrated through the fabricated membranes (NPG-pTD1, NPG-pTD2, and NPG-pTD3), which were then dried at 70 °C overnight.

Characterization of synthesized nanosheets and membranes

An atomic force microscope (AFM Bruker Dimension Icon with ScanAsyst, Bruker, Germany) was used to measure the thickness of the GO and NPG nanosheets in tapping mode. The dispersed solutions of GO or HG were applied to a mica substrate from Ted Pella, Inc. in Redding, California, and allowed to air dry[53]. The high-resolution images of the GO and HG nanosheets were captured by transmission electron microscopy (TEM, Titan, Thermo Fisher Scientific, 300 kV). High-resolution scanning electron microscopy (SEM) was also used to examine the manufactured membranes' surfaces and cross-sectional morphologies (FEI Nova NanoSEM 650). The sample preparation for SEM included the deposition of a 5 nm gold-palladium coating layer on all membrane samples to avoid charging and improve imaging quality. Additionally, samples were frozen and quickly fractured as part of the freeze–fracture method, which was used to prepare samples for cross-sectional analysis. All the prepared samples were positioned in the SEM stubs using adhesive carbon tape[54].

Table 1 | Comparison of the performance profile of NPG-pTD membrane for oil-water separation with other work in the literature

Membrane composite	Oil rejection (%)	Flux (LMH)	Ref.
N-oxide zwitterionic polymer	99	1121	[51]
PSF/MWCNTs-OH	90	118	[50]
PEI/PHMB-CuO	97	193	[49]
Polyacrylic acid/PVDF	90	300	[48]
Free-standing SBG	97	625	[12]
PBI/GO	99.9	91	[13]
Titanate nanofibers/SiO₂	99.5	1600	[47]
NPG-pTD	97	2490	This work

PSF polysulfone, *PEI* polyethylenimine, *dPHMB* polyhexamethylene biguanide, *eCuO* copper oxide, *fPVDF* polyvinylidene fluoride, *gSBG* sodium-bentonite-fabricated graphene, *hPBI* poly-benzimidazole, *iGO* graphene oxide, *jSiO2* silicon dioxide, *kNPG* nanoporous graphene, *lpTD* poly tannic acid/dopamine.
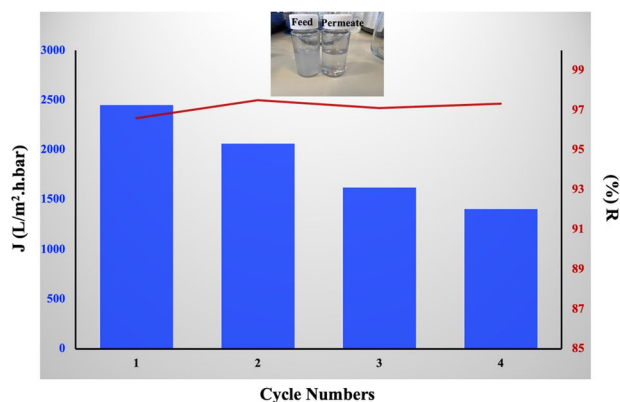
Fig. 11 | Membrane reusability. Oil rejection and flux profiles of the NPG-pTD3 membrane in four cycles.

Energy dispersive X-ray (EDS) spectroscopy was used to trace the elements present in the synthesized membranes. Several acceleration voltages were used. Additionally, ATR-FT-IR spectroscopy (Bruker Vertex 80 v spectrometer, wavelength = 400–4000 cm^{-1} and precision = 4 cm^{-1}) was used to examine the surface functional groups of the membranes. All samples were scanned 64 times[55]. The X-ray diffraction (XRD) analysis was performed using Cu Kα radiation (λ = 0.154 nm, PANalytical Empyrean) to evaluate the manufactured membranes as well. All measurements were made using an angular (2θ) range of 5° to 70° while the XRD was run at 40 kV tension and 35 mA current. The Zetasizer 7.13 (Malvern Panalytical Instruments Ltd.) was used to analyze the surface charge of the nanomaterial in DI water (0.1 mg mL^{-1}) at a pH of 6.4 ± 0.2. Water contact angle (WCA, Krüss GmbH's Drop Shape Analyzer, DSA), which uses the sessile drop technique to deposit water droplets on the top of the manufactured membranes at room temperature, was employed to determine the hydrophilicity nature of the membranes. The test was conducted five seconds before water droplets (5 μL) were deposited on the membrane surface, and the average of five measurements was then computed.

Performance analysis of the manufactured membranes

A dead-end vacuum filtration system (area = 14.5 cm^2 under pressure (0.8 bar) and 200 mL feed solution) was employed at room temperature to test the permeance and surfactant stabilized oil/water emulsion separation capability of the manufactured membranes. The SDS surfactant and oil (1000 ppm) were initially added into DI water consecutively with a mass ratio of 0.15 (surfactant/oil) under mechanical blending. To achieve the initial emulsification, the combination was then sonicated in a Branson ultrasonic bath for two hours at a power level of 70 Watts. To intensify the emulsification, this emulsion was exposed to tip sonication (Vibra CellTM) at 750 Watts for 15 min.

Prior to filtration experiments, the membranes were soaked in the feed solutions. The permeance measurement started by stabilizing the obtained values under one bar, followed by recording the values every 10 min at 0.8 bars. A UV–vis spectrophotometer was used to determine the oil concentration (Shimadzu, Japan). The average of three measurements was used to create all the statistics, according to Eqs. (1) and (2), the permeance (J, L m^{-2} h^{-1} bar^{-1}) in addition to rejection (R%) were determined, respectively.

$$J = \frac{V}{A\Delta tP} \tag{1}$$

$$R = 1 - \frac{Cp}{Cf} \times 100\% \tag{2}$$

where P (0.8 bar) is the applied pressure, Δt (h) is the permeate duration, V (L) is the volume of permeated water, A (m^2) is the effective membrane area,

Cp and Cf refer to the concentrations of the permeate and feed solutions, correspondingly.

Data availability

The data analyzed during this study are available from the corresponding author upon request.

References
1. Anton, N., Benoit, J. P. & Saulnier, P. Design and production of nanoparticles formulated from nano-emulsion templates-a review. *J. Control. Release* **128**, 185–199 (2008).
2. Wooster, T. J., Golding, M. & Sanguansri, P. Impact of oil type on nanoemulsion formation and Ostwald ripening stability. *Langmuir* **24**, 12758–12765 (2008).
3. McClements, D. J. Nanoemulsions versus microemulsions: terminology, differences, and similarities. *Soft Matter* **8**, 1719–1729 (2012).
4. Jackson, M. et al. Comprehensive review of several surfactants in marine environments: fate and ecotoxicity. *Environ. Toxicol. Chem.* **35**, 1077–1086 (2016).
5. Lechuga, M., Fernández-Serrano, M., Jurado, E., Núñez-Olea, J. & Ríos, F. Acute toxicity of anionic and non-ionic surfactants to aquatic organisms. *Ecotoxicol. Environ. Saf.* **125**, 1–8 (2016).
6. Tadros, T., Izquierdo, P., Esquena, J. & Solans, C. Formation and stability of nano-emulsions. *Adv. Colloid Interface Sci.* **108–109**, 303–318 (2004).
7. Hu, J., Li, X. & Dong, J. Development of highly efficient oil-water separation carbon nanotube membranes with stimuli-switchable fluxes. *ACS Omega* **3**, 6635–6641 (2018).
8. Deng, Y., Dai, M., Wu, Y. & Peng, C. Emulsion system, demulsification and membrane technology in oil–water emulsion separation: a comprehensive review. *Crit. Rev. Environ. Sci. Technol.* **53**, 1254–1278 (2022).
9. Solomon, B. R., Hyder, M. N. & Varanasi, K. K. Separating oil-water nanoemulsions using flux-enhanced hierarchical membranes. *Sci. Rep.* **4**, 1–6 (2014).
10. Hegab, H. M. et al. Mechanistic insights into the selective mass-transport and fabrication of holey graphene-based membranes for water purification applications. *Chem. Eng. J.* **431**, 134248 (2022).
11. Rasouli, S., Rezaei, N., Hamedi, H., Zendehboudi, S. & Duan, X. Superhydrophobic and superoleophilic membranes for oil-water separation application: a comprehensive review. *Mater. Des.* **204**, 109599 (2021).
12. Dhumal, P. S., Khose, R. V., Wadekar, P. H., Lokhande, K. D. & Some, S. Graphene-bentonite supported free-standing, flexible membrane with switchable wettability for selective oil–water separation. *Sep. Purif. Technol.* **266**, 118569 (2021).
13. Alammar, A., Park, S. H., Williams, C. J., Derby, B. & Szekely, G. Oil-in-water separation with graphene-based nanocomposite membranes for produced water treatment. *J. Membr. Sci.* **603**, 118007 (2020).
14. Bondarde, M. P., Bhakare, M. A., Dhumal, P. S., Lokhande, K. D. & Some, S. Synthesis of biowaste derived ultra-light spongy material for the studies of effective removal of oil, organic solvent and selective dye pollutant from waste stream. *Biocatal. Agric. Biotechnol.* **43**, 102426 (2022).
15. Joshi, R. K. et al. Precise and ultrafast molecular sieving through graphene oxide membranes. *Science* **343**, 752–754 (2014).
16. Hegab, H. M. & Zou, L. Graphene oxide-assisted membranes: Fabrication and potential applications in desalination and water purification. *J. Memb. Sci.* **484**, 95–106 (2015).
17. Gao, P., Liu, Z., Sun, D. D. & Ng, W. J. The efficient separation of surfactant-stabilized oil–water emulsions with a flexible and

superhydrophilic graphene–TiO2 composite membrane. *J. Mater. Chem. A* **2**, 14082–14088 (2014).

18. Hu, X. et al. The improved oil/water separation performance of graphene oxide modified Al2O3 microfiltration membrane. *J. Memb. Sci.* **476**, 200–204 (2015).

19. Liu, Z. et al. A mussel inspired highly stable graphene oxide membrane for efficient oil-in-water emulsions separation. *Sep. Purif. Technol.* **199**, 37–46 (2018).

20. Hegab, H. M. et al. Ultrafast aquaporin-like multi-functionalized holey graphene membrane with tripartite nanochannels for organic solvent nanofiltration. *Chem. Eng. J.* **450**, 138033 (2022).

21. Hegab, H. M. et al. Designing of amino silica covalently functionalized carboxylic multi-wall carbon nanotubes-based polyethersulfone membranes for enhancing oily wastewater treatment. *J. Environ. Chem. Eng.* **10**, 108667 (2022).

22. Chen, L. et al. Ion sieving in graphene oxide membranes via cationic control of interlayer spacing. *Nature* **550**, 380–383 (2017).

23. Yèagle, P. L. Lipid regulation of cell membrane structure and function. *FASEB J.* **3**, 1833–1842 (1989).

24. Lee, C. S. et al. Facilitated water transport through graphene oxide membranes functionalized with aquaporin-mimicking peptides. *Adv. Mater.* **30**, 1705944 (2018).

25. Park, H. et al. Large scale synthesis and light emitting fibers of tailor-made graphene quantum dots. *Sci. Rep.* **5**, 1–9 (2015).

26. Han, T. H., Huang, Y. K., Tan, A. T. L., Dravid, V. P. & Huang, J. Steam etched porous graphene oxide network for chemical sensing. *J. Am. Chem. Soc.* **133**, 15264–15267 (2011).

27. Lee, D. W. et al. Highly controllable transparent and conducting thin films using layer-by-layer assembly of oppositely charged reduced graphene oxides. *J. Mater. Chem.* **21**, 3438–3442 (2011).

28. Wang, S. et al. Band-like transport in surface-functionalized highly solution-processable graphene nanosheets. *Adv. Mater.* **20**, 3440–3446 (2008).

29. Yang, H. et al. Covalent functionalization of chemically converted graphene sheets via silane and its reinforcement. *J. Mater. Chem.* **19**, 4632–4638 (2009).

30. Chen, X. et al. Reduced holey graphene oxide membranes for desalination with improved water permeance. *ACS Appl. Mater. Interfaces* **12**, 1387–1394 (2020).

31. Cattley, C. A. et al. Colloidal synthesis of lead oxide nanocrystals for photovoltaics. *ChemComm* **46**, 2802–2804 (2010).

32. Wang, G. et al. Synthesis of enhanced hydrophilic and hydrophobic graphene oxide nanosheets by a solvothermal method. *Carbon* **47**, 68–72 (2009).

33. Xia, S., Yao, L., Zhao, Y., Li, N. & Zheng, Y. Preparation of graphene oxide modified polyamide thin film composite membranes with improved hydrophilicity for natural organic matter removal. *Chem. Eng. J.* **280**, 720–727 (2015).

34. Yin, J., Zhu, G. & Deng, B. Graphene oxide (GO) enhanced polyamide (PA) thin-film nanocomposite (TFN) membrane for water purification. *Desalination* **379**, 93–101 (2016).

35. Wang, J. et al. Graphene oxide as an effective barrier on a porous nanofibrous membrane for water treatment. *ACS Appl. Mater. Interfaces* **8**, 6211–6218 (2016).

36. Choi, S. H. et al. Properties of graphene/waterborne polyurethane nanocomposites cast from colloidal dispersion mixtures. *J. Macromol. Sci. B* **51**, 197–207 (2011).

37. Reddy, K. R., Sin, B. C., Ryu, K. S., Noh, J. & Lee, Y. In situ self-organization of carbon black–polyaniline composites from nanospheres to nanorods: Synthesis, morphology, structure and electrical conductivity. *Synth. Met.* **159**, 1934–1939 (2009).

38. Son, D. R., Raghu, A. V., Reddy, K. R. & Jeong, H. M. Compatibility of thermally reduced graphene with polyesters. *J. Macromol. Sci. B* **55**, 1099–1110 (2016).

39. Johannsen, I. et al. Electrical conductivity of melt-spun thermoplastic poly(hydroxy ether of bisphenol A) fibres containing multi-wall carbon nanotubes. *Polymers* **97**, 80–94 (2016).

40. Xu, L. Q., Neoh, K. G. & Kang, E. T. Natural polyphenols as versatile platforms for material engineering and surface functionalization. *Prog. Polym. Sci.* **87**, 165–196 (2018).

41. Costa, M. N. et al. A low cost, safe, disposable, rapid and self-sustainable paper-based platform for diagnostic testing: lab-on-paper. *Nanotechnology* **25**, 094006 (2014).

42. Ramesh, S., Leen, K. H., Kumutha, K. & Arof, A. K. FTIR studies of PVC/PMMA blend based polymer electrolytes. *Spectrochim. Acta A Mol. Biomol. Spectrosc.* **66**, 1237–1242 (2007).

43. Muñoz, E. M. et al. The relevance of carbohydrate hydrogen-bonding cooperativity effects: a cooperative 1,2-trans-diaxial diol and amido alcohol hydrogen-bonding array as an efficient carbohydrate-phosphate binding motif in nonpolar media. *Chemistry* **8**, 1908–1914 (2002).

44. Chen, X., Liu, G., Zhang, H. & Fan, Y. Fabrication of graphene oxide composite membranes and their application for pervaporation dehydration of butanol. *Chin. J. Chem. Eng.* **23**, 1102–1109 (2015).

45. Cote, L. J., Kim, J., Zhang, Z., Sun, C. & Huang, J. Tunable assembly of graphene oxide surfactant sheets: wrinkles, overlaps and impacts on thin film properties. *Soft Matter* **6**, 6096–6101 (2010).

46. Goh, K. et al. Graphene oxide as effective selective barriers on a hollow fiber membrane for water treatment process. *J. Membr. Sci.* **474**, 244–253 (2015).

47. Elshorafa, R., Saththasivam, J., Liu, Z. & Ahzi, S. Efficient oil/saltwater separation using a highly permeable and fouling-resistant all-inorganic nanocomposite membrane. *Environ. Sci. Pollut. Res.* **27**, 15488–15497 (2020).

48. Wang, L., Pan, K., Li, L. & Cao, B. Surface hydrophilicity and structure of hydrophilic modified PVDF membrane by nonsolvent induced phase separation and their effect on oil/water separation performance. *Ind. Eng. Chem. Res.* **53**, 6401–6408 (2014).

49. Sri Abirami Saraswathi, M. S. et al. Highly permeable, antifouling and antibacterial poly(ether imide) membranes tailored with poly(hexamethylenebiguanide) coated copper oxide nanoparticles. *Mater. Chem. Phys.* **240**, 122224 (2020).

50. Santosh, V. et al. Development of hydroxyl and carboxylic acid functionalized CNTs–polysulphone nanocomposite fouling-resistant ultrafiltration membranes for oil–water separation. *Bull. Mater. Sci.* **43**, 1–12 (2020).

51. Yang, J., Lin, L., Tang, F. & Zhao, J. Superwetting membrane by co-deposition technique using a novel N-oxide zwitterionic polymer assisted by bioinspired dopamine for efficient oil–water separation. *Sep. Purif. Technol.* **318**, 123965 (2023).

52. Marcano, D. C. et al. Improved synthesis of graphene oxide. *ACS Nano* **4**, 4806–4814 (2010).

53. Hegab, H. M. et al. Fine-tuning the surface of forward osmosis membranes via grafting graphene oxide: performance patterns and biofouling propensity. *ACS Appl. Mater. Interfaces* **7**, 18004–18016 (2015).

54. Hegab, H. M., Wimalasiri, Y., Ginic-Markovic, M. & Zou, L. Improving the fouling resistance of brackish water membranes via surface modification with graphene oxide functionalized chitosan. *Desalination* **365**, 99–107 (2015).

55. Hegab, H. M. et al. Effective in-situ chemical surface modification of forward osmosis membranes with polydopamine-induced graphene oxide for biofouling mitigation. *Desalination* **385**, 126–137 (2016).

Acknowledgements

Author contributions
Hanaa M. Hegab: Conceptualization, Methodology, Preparations, Characterizations, Writing an original draft, Review & Editing. Ahmed Elmekawy: Conceptualization, Methodology, Characterizations, Writing an original draft, Review & Editing (co-first author). Cyril Aubry: Characterizations. Parashuram Kallem: Review & Editing. Vijay S. Wadi: Review & Editing. Fawzi Banat: Review & Editing. Shadi W. Hasan: Conceptualization, Validation, Resources, Review & Editing, Administration.

Competing interests
The authors declare no competing interests.

Additional information
Correspondence and requests for materials should be addressed to Hanaa M. Hegab or Shadi W. Hasan.

Reprints and permissions information is available at http://www.nature.com/reprints

Publisher's note Springer Nature remains neutral with regard to jurisdictional claims in published maps and institutional affiliations.